



**PEG-b-AGE Polymer Coated Magnetic Nanoparticle Probes  
with Facile Functionalization and Anti-fouling Properties for  
Reducing Non-specific Uptake and Improving Biomarker  
Targeting**

Journal:	<i>Journal of Materials Chemistry B</i>
Manuscript ID:	TB-ART-11-2014-001828.R1
Article Type:	Paper
Date Submitted by the Author:	19-Feb-2015
Complete List of Authors:	<p>Li, Yuancheng; Emory University School of Medicine, Department of Radiology and Imaging Sciences          Lin, Run; Emory University School of Medicine, Department of Radiology and Imaging Sciences; the First Affiliated Hospital of Sun Yat-Sen University, Department of Radiology          Wang, Liya; Emory University, Department of Radiology and Imaging Sciences          Huang, Jing; Emory University, Department of Radiology and Imaging Sciences          Wu, Hui; Emory University School of Medicine, Department of Radiology and Imaging Sciences          Chen, Guojun; Emory University School of Medicine, Department of Radiology and Imaging Sciences          Zhou, zhengyang; Emory University School of Medicine, Department of Radiology and Imaging Sciences; Nanjing University, Department of Radiology          MacDonald, Tobey; Emory University School of Medicine, Department of Pediatrics          Yang, Lily; Emory University School of Medicine, Department of Surgery          Mao, Hui; Emory University, Department of Radiology and Imaging Sciences</p>

## ARTICLE

# PEG-*b*-AGE Polymer Coated Magnetic Nanoparticle Probes with Facile Functionalization and Anti-fouling Properties for Reducing Non-specific Uptake and Improving Biomarker Targeting

Cite this: DOI: 10.1039/x0xx00000x

Received 00th January 2012,  
Accepted 00th January 2012

DOI: 10.1039/x0xx00000x

[www.rsc.org/](http://www.rsc.org/)Yuancheng Li,<sup>a†</sup> Run Lin,<sup>a,b†</sup> Liya Wang,<sup>a</sup> Jing Huang,<sup>a</sup> Hui Wu,<sup>a</sup> Guojun Cheng,<sup>a</sup> Zhengyang Zhou,<sup>a,c</sup> Tobey MacDonald,<sup>a</sup> Lily Yang<sup>e</sup> and Hui Mao<sup>a</sup>

Non-specific surface adsorption of bio-macromolecules (e.g. proteins) on nanoparticles, known as biofouling, and the uptake of nanoparticles by the mononuclear phagocyte system (MPS) and reticuloendothelial system (RES) lead to substantial reduction in the efficiency of target-directed imaging and delivery in biomedical applications of engineered nanomaterials *in vitro* and *in vivo*. In this work, a novel copolymer consisting of blocks of poly ethylene glycol and allyl glycidyl ether (PEG-*b*-AGE) was developed for coating magnetic iron oxide nanoparticles (IONPs) to reduce non-specific protein adhesion that leads to formation of “protein corona” and uptake by macrophages. The facile surface functionalization was demonstrated by using targeting ligands of a small peptide of RGD or a whole protein of transferrin (Tf). The PEG-*b*-AGE coated IONPs exhibited anti-biofouling properties with significantly reduced protein corona formation and non-specific uptake by macrophages before and after the surface functionalization, thus improving targeting of RGD-conjugated PEG-*b*-AGE coated IONPs to integrins in U87MG glioblastoma and MDA-MB-231 breast cancer cells that overexpress  $\alpha_v\beta_3$  integrins, and Tf-conjugated PEG-*b*-AGE coated IONPs to transferrin receptor (TfR) in D556 and Daoy medulloblastoma cancer cells with high overexpression of transferrin receptor, compared to respective control cell lines. Magnetic resonance imaging (MRI) of cancer cells treated with targeted IONPs with or without anti-biofouling PEG-*b*-AGE coating polymers demonstrated the target specific MRI contrast change using anti-biofouling PEG-*b*-AGE coated IONP with minimal off-targeted background compared to the IONPs without anti-biofouling coating, promising the highly efficient active targeting of nanoparticle imaging probes and drug delivery systems and potential applications of imaging quantification of targeted biomarkers.

## Introduction

While engineered nanomaterials, particularly nanoparticles, have provided many novel tools and applications in molecular diagnosis, biomarker targeted imaging and delivery of therapy in the past decade,<sup>1-8</sup> a well-recognized major obstacle is the non-specific interaction between nanoparticles and endogenous biological materials. This biofouling effect leads to changes in the nanoparticle surface and functional properties and subsequent nanoparticle aggregation, as well as undesirable cellular uptake and immune system response.<sup>9-11</sup> For *in vivo* applications after systemic administration and *in vitro* applications with tissue and plasma samples, nanoparticles are subject to immediate interactions with bio-macromolecules, such as proteins in the blood, interstitial fluid, and cellular cytoplasm.<sup>12</sup> The rapid non-specific adsorption of

proteins results in the formation of a protein layer, or protein corona, on the nanoparticle surface.<sup>13,14</sup> The presence of the protein corona is responsible for the fast clearance of nanoparticles by the mononuclear phagocyte system (MPS), particularly macrophages,<sup>8</sup> and the reticuloendothelial system (RES), such as the liver, spleen, and lung.<sup>15-19</sup> The biofouling or surface adsorption of bio-macromolecules and non-specific uptake of nanoparticles by normal tissue and cells cause the substantial reduction in targeting efficiency and the off-target background signal in imaging,<sup>20</sup> as well as unwanted toxicity to the normal tissues in biomarker targeted drug delivery applications. In the effort to develop anti-biofouling materials, poly ethylene glycol (PEG), polysaccharides and zwitterionic polymers have been investigated.<sup>8,21-24</sup> Although these materials have shown the capability of reducing biofouling given their inert structures, the facile functionalization of these materials

for introducing targeting ligands is challenging.<sup>24-26</sup> Currently, the most commonly used strategy to overcome non-specific protein adsorption and cell uptake is to graft PEG onto the nanoparticle surface,<sup>26-31</sup> because PEG facilitates the formation of a hydrate film around the particle through hydrogen bonding with water, which attenuates the protein interactions, cell uptake,<sup>27</sup> and immunogenic response.<sup>32-40</sup> In order to immobilize targeting ligands onto nanoparticles with PEG based coating, the typical approach is to introduce additional moieties that contain reactive groups (e.g. -NH<sub>2</sub> or -COOH) for functionalization.<sup>24,29-31</sup> Since surface charge may promote the phagocytosis process,<sup>26,41-44</sup> the surface charge introduced from the reactive groups would “offset” the anti-biofouling effect from PEG. Hence, a coating material that bears reactive functional groups yet still exhibits anti-biofouling property is desirable.

Herein, we report the development of a novel anti-biofouling amphiphilic diblock coating polymer that incorporates aminated hydrophilic PEG chains with hydrophobic allyl glycidyl ether (AGE) moieties, and can potentially control functional ligand density of the coating polymer during the polymerization of AGE through anionic ring-opening of the glycidyl group.<sup>45</sup> The allyl group of AGE can be utilized for the attachment of other functional segments, e.g. anchoring groups, through the highly efficient and regioselective thiol-ene coupling reaction with great tolerance toward a variety of functional groups.<sup>45,46</sup> This PEG-*b*-AGE copolymer utilizes the reactive trimethoxysilane group in one segment to “anchor” on the surface of highly size uniformed magnetic iron oxide nanoparticles (IONPs) obtained from thermo-decomposition, enabling coating and stabilization of the nanoparticles for further applications in physiological conditions.

## Results and discussion

### Synthesis and characterization of PEG-*b*-AGE coating polymer

The PEG-*b*-AGE diblock polymer was obtained successfully with the procedure described in Scheme 1. The anionic ring opening employed in the synthesis of NH<sub>2</sub>-PEG-AGE 2 provides good control over the number of AGE molecules attached to the PEG chain with Low PDIs.<sup>46</sup> The number of AGE moieties in each PEG-*b*-AGE polymer would further affect the surface charge and ligand density after the nanoparticle is coated with the PEG-*b*-AGE polymer. Consequently, the anionic ring opening step would allow us to

attenuate the surface property of the PEG-*b*-AGE coated nanoparticles. The thiol-ene coupling reaction between the NH<sub>2</sub>-PEG-AGE 2 and the 3-mercaptopropyl trimethoxysilane took place in a highly regioselective fashion in the presence of AIBN. The radical addition of the thiol group from the 3-mercaptopropyl trimethoxysilane to the allyl group from the NH<sub>2</sub>-PEG-AGE 2 led to the PEG-*b*-AGE polymer 3 as the only product. The trimethoxysilane group in 3 functions as an “anchor” that attaches the polymer onto the surface of IONPs, while the -NH<sub>2</sub> group in the other segment enables the coupling with the selected functional modality.

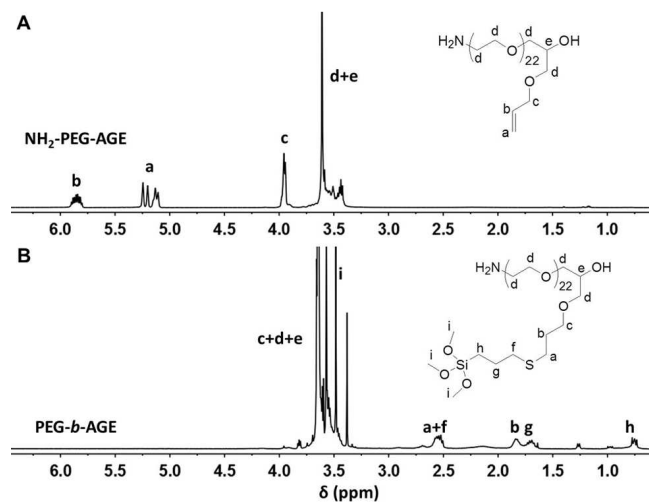
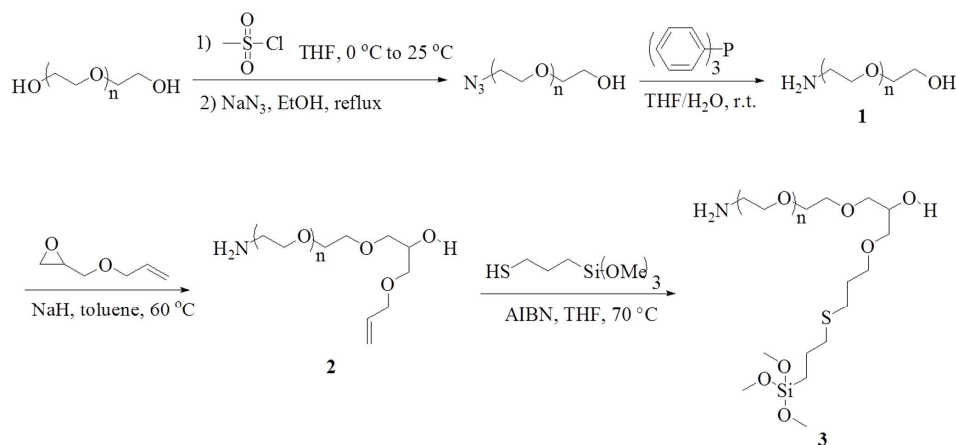


**Figure 1.** <sup>1</sup>H NMR spectra of (A) NH<sub>2</sub>-PEG-AGE, and (B) PEG-*b*-AGE. Samples were dissolved in CDCl<sub>3</sub>.

**Figure 1** shows <sup>1</sup>H NMR spectra of the precursor NH<sub>2</sub>-PEG-AGE (**Figure 1A**), and the polymer PEG-*b*-AGE (**Figure 1B**), respectively. In the spectra, the resonance at  $\delta \approx 5.85$  is arising from the proton at position b (H-C=C) and two adjacent peaks at 5.22 ppm are resonances from protons at position a (C=C-H<sub>2</sub>) (**Figure 1A**). After the C=C was converted to C-C, these peaks shifted to  $\delta \approx 2.54$  and 1.84 ppm (peaks a and b in **Figure 1B**), indicating the successful thiol-ene coupling. With the conversion of C=C to C-C, the de-shielding effect provided by the C=C to the neighbouring protons diminished, making the neighbouring proton signal at  $\delta \approx 3.95$  ppm (peak c in **Figure 1A**) shift upfield (right, lower ppm), overlapping with proton



**Scheme 1.** Synthesis of the coating polymer PEG-*b*-AGE 3.

signals from the PEG chain (peak c in **Figure 1B**). After coupling with 3-mercaptopropyl trimethoxysilane, three new peaks at  $\delta \approx 2.54$ ,  $\delta \approx 1.69$ , and  $\delta \approx 0.75$  ppm (peaks f, g, and h in **Figure 1B**) emerged, which can be ascribed to the three methylene groups from the 3-mercaptopropyl trimethoxysilane. The characteristic peak of protons from trimethoxysilane (peak i in **Figure 1B**) can also be found at  $\delta \approx 3.50$  ppm. The ratio of integration numbers of peak a, d, and e in **Figure 1A** indicated only one AGE molecule was attached to the polymer. The average molecular weight of  $\text{NH}_2$ -PEG-AGE **2** was found to be 1034 g/mol in the MALDI mass spectrometry, confirming that each polymer molecule contains one AGE segment.

### Coating IONPs with Diblock PEG-*b*-AGE polymer

After coating the hydrophobic oleic acid attached IONPs with PEG-*b*-AGE polymer, the hydrophobic block of the coating polymer collapsed onto the surface of IONPs once exposed to water, resulting in a self-assembled hydrophobic layer to protect the iron oxide nanocrystal core. Meanwhile, the outer layer formed from the hydrophilic block led the resultant PEG-*b*-AGE polymer coated IONPs to be mono-dispersed in water, preventing the particles from aggregation. As shown in the TEM images (**Figure 2A and B**), PEG-*b*-AGE polymer coated IONPs with core diameters of both 10 nm and 20 nm were highly mono-dispersed in water. A thin polymer layer around the core of the IONPs can be observed in the TEM images. The thickness of the coating polymer layer is estimated to be 2.5 nm based on the measurements from TEM images. The average hydrodynamic diameters of the PEG-*b*-AGE polymer coated IONPs with core diameters of 10 nm and 20 nm were measured at 22.4 nm and 30.5 nm, respectively (**Table 1**). The polydispersity indexes (PDIs) are 0.213 for a nanoparticle with a core size of 10 nm and 0.225 for that with core size of 20 nm. The low PDI values of the hydrodynamic diameter measurements indicate narrow size distributions of PEG-*b*-AGE polymer coated IONPs.<sup>47</sup> The number of surface  $-\text{NH}_2$  groups for each particle was determined using the ninhydrin colorimetric method, and found to be  $606 \pm 84$  and  $1720 \pm 214$  for the PEG-*b*-AGE polymer coated IONP with core diameters of 10 nm and 20 nm respectively (**Table 1**).

### Conjugation of targeting ligands to the PEG-*b*-AGE polymer coated IONPs

Biomarker-targeted application is a major focus of nanomaterial development with a wide variety of targeting ligands, including small molecules, peptides, proteins, antibodies and their fragments, polysaccharides, and aptamers, being used and explored.<sup>25,48,49</sup> The conjugation reaction conditions for assembling ligands to the nanoparticle surface have to be as mild and biocompatible as possible to maintain the biological functions of targeting ligands. To

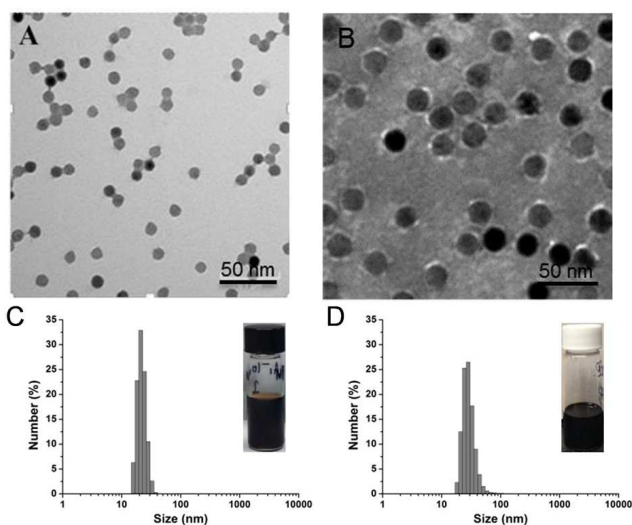


**Figure 2.** TEM image of (A) PEG-*b*-AGE polymer coated IONP (with a core diameter of 10 nm) in water, and (B) PEG-*b*-AGE coated IONP (with a core diameter of 0 nm) in water. Hydrodynamic diameter distribution of (C) PEG-*b*-AGE polymer coated IONP (with a core diameter of 10 nm), and (D) PEG-*b*-AGE polymer coated IONP (with a core diameter of 20 nm) measured by DLS. The inset of C is a photograph of PEG-*b*-AGE polymer coated IONP (with a core diameter of 10 nm) dispersed in water. The inset of D is a photograph of PEG-*b*-AGE coated IONP (with a core diameter of 20 nm) dispersed in water.

enable a robust capability of conjugating various targeting moieties on the developed PEG-*b*-AGE polymer coated IONP, the “click” reaction between the thiol group and maleimide was used for the conjugation of ligands because of its high efficiency, good control of functional groups used for conjugation, and water compatibility.<sup>45</sup>

A small peptide RGD and a large protein transferrin (Tf), both frequently used to test nanoparticle targeting of overexpressed integrin or transferrin receptor (TfR),<sup>50-53</sup> were used as the model ligands to demonstrate the robustness of the conjugations of different classes of targeting ligands to the PEG-*b*-AGE polymer coated IONP. The successful attachments of the targeting ligands to the PEG-*b*-AGE polymer coated IONP were first confirmed by the observed increase in hydrodynamic diameters and change of  $\zeta$ -potentials of the nanoparticle after conjugations (**Table 1**).

PEG-*b*-AGE polymer coated IONPs with  $-\text{NH}_2$  group functionalized have slightly positive surface potential due to the presence of  $-\text{NH}_2$  groups. The surface charge of the nanoparticle became negative as the result of the neutralization of  $-\text{NH}_2$  groups

**Table 1.** Hydrodynamic sizes and surface charges of PEG-*b*-AGE polymer coated IONPs and ligand conjugated IONPs.

		PEG- <i>b</i> -AGE coated IONP	RGD-IONP	Tf-IONP
Particle with 10 nm core	$\zeta$ – potential (mV)	$1.85 \pm 0.42$	$-3.30 \pm 1.25$	$-6.69 \pm 0.84$
	$D_H$ (nm)	$22.4 \pm 0.6$	$24.7 \pm 4.3$	$44.0 \pm 7.3$
Particle with 20 nm core	$\zeta$ – potential (mV)	$17.08 \pm 2.06$	$-8.87 \pm 0.06$	$-24.60 \pm 3.82$
	$D_H$ (nm)	$30.5 \pm 1.6$	$33.6 \pm 6.4$	$48.7 \pm 6.9$

when ligands were covalently conjugated. The change of  $\zeta$ -potential values after conjugations was in accordance with previously reported study.<sup>28</sup> The greater absolute values of  $\zeta$ -potential for particle with 20 nm core size comparing to the one with 10 nm core can be ascribed as a higher number of targeting ligands conjugated on the larger particle which has more  $-NH_2$  groups. This hypothesis was confirmed by the  $-NH_2$  group quantification using ninhydrin. Since RGD is a small peptide that should not expand the hydrodynamic diameters significantly, the hydrodynamic diameters of the particles (with core diameters of both 10 nm and 20 nm) slightly increased after conjugation with RGD. On the other hand, the conjugation with a large protein, such as transferrin (80 kDa), led to a significant increase in the hydrodynamic diameter. The average number of transferrin molecules attached to each nanoparticle is 2.4 estimated by comparing the protein concentration to the IONP concentration of the Tf-IONP. Since RGD has an aspartic acid (asp) residue that contains one COOH group, the average number of conjugated RGD can be determined by quantifying the number of COOH groups. It was found that  $456 \pm 60$  and  $1447 \pm 105$  RGD peptides were conjugated to the IONPs with core diameters of 10 nm and 20 nm, respectively.

### Reduced protein adsorption on PEG-*b*-AGE polymer coated IONPs

In soluble media such as blood, serum proteins can non-specifically adsorb onto the surface of nanoparticles and form stable protein corona very rapidly upon contacting nanoparticles.<sup>25,54,55</sup> To test whether PEG-*b*-AGE polymer can reduce the formation of protein corona around the coated IONPs, the nanoparticles were incubated with the protein containing media for one hour to allow the adsorption of proteins and formation of the corona. Given the better efficiency of magnetic separation used in this experiment, the particles with 20 nm core diameter were used. After the surface protein corona was washed off by KCl solution, the protein concentrations in the wash-off solution were measured using the bicinchoninic acid (BCA) protein assay. As shown in **Figure 3A**, for the PEG-*b*-AGE polymer coated IONP (with a core diameter of 20 nm), the protein concentrations of the wash-off solutions were 47  $\mu\text{g/mL}$  for particle in FBS, and 97  $\mu\text{g/mL}$  in human plasma. In comparison, iron oxide nanoparticles coated with conventional amphiphilic triblock copolymer (SHP with a core diameter of 20 nm), which has  $2012 \pm 162$  -COOH groups on the surface, had protein concentrations in the washed-off solution of 623  $\mu\text{g/mL}$  in FBS, and 792  $\mu\text{g/mL}$  in human plasma. The significantly reduced level of proteins adsorbed on the surface of PEG-*b*-AGE polymer coated IONP clearly indicate efficiently reducing the non-specific protein adsorption onto the nanoparticle surface, suggesting the excellent anti-biofouling property of the developed PEG-*b*-AGE coating polymer.

Since the formation of corona can change the size, shape and surface charge of nanoparticles<sup>56,57</sup> the anti-biofouling property of PEG-*b*-AGE polymer coated IONPs was examined by measuring the size stability in protein containing medium. The hydrodynamic size of PEG-*b*-AGE polymer coated IONP (with a core diameter of 20 nm) demonstrated remarkable stability against the protein adsorption in 100% FBS within 24 hours with only slight change of the hydrodynamic size, as shown in **Figure 3B**, suggesting that the presence of the proteins in the media did not change the surface properties of the PEG-*b*-AGE polymer coated IONPs significantly. In contrast, the hydrodynamic size of SHP-20 exhibited substantial increase in hydrodynamic size from 45 nm to 130 nm over a period of 24 hour incubation when exposed to only 10% FBS. These results are in great accordance with the results of the surface protein

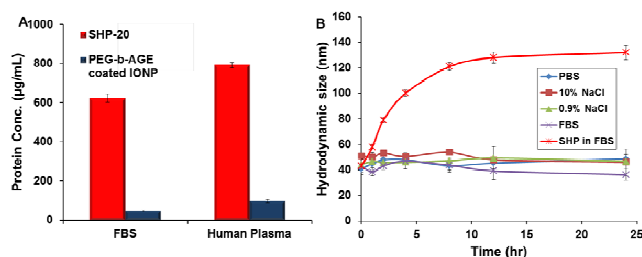


**Figure 3.** (A) Surface protein corona formation measurement of commercially available amphiphilic polymer coated SHP-20 (with a core diameter of 20 nm) and PEG-*b*-AGE polymer coated IONP quantified by BCA protein assay. (B) Stability of PEG-*b*-AGE polymer coated IONP (with a core diameter of 20 nm) in PBS, 10% (w/v) NaCl aqueous solution, 0.9% NaCl aqueous solution, and 100% FBS, compared with amphiphilic triblock polymer coated SHP-20 in 10% FBS at the Fe concentration of 0.1 mg/mL.

corona measurement, suggesting the anti-biofouling properties of the PEG-*b*-AGE polymer coated IONPs. Although a careful and systematic investigation may be needed to elucidate the mechanism, it is considered that AGE moieties may contribute to the enhanced anti-biofouling property of PEG-*b*-AGE polymer coated IONP. The hydrophobic AGE layer provides extra stability of the polymer coating over simple PEGylation, which can be replaced by biomolecules under physiological condition.<sup>58</sup> As a result, PEG-*b*-AGE polymer coating may have a sustained anti-biofouling effect.

Worth noting, PEG-*b*-AGE polymer coated IONP also exhibited good stability in PBS and 10% NaCl solutions (shown in **Figure 3B**), which provided high surface charge and ionic strength that may lead to particle aggregation.<sup>48</sup> The PEG-

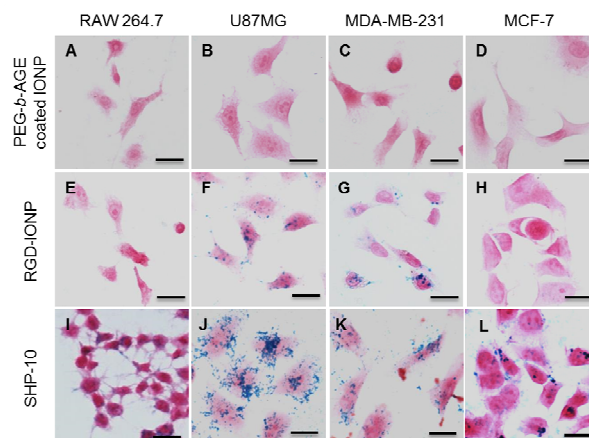


**Figure 4.** Prussian blue stained images of PEG-*b*-AGE polymer coated IONP (with core a diameter of 10 nm) incubated with (A) RAW264.7 macrophage cells, (B) U87MG glioblastoma cells, (C) MDA-MB-231 breast cancer cells, (D) MCF-7 breast cancer cells; and RGD-IONP (with a core diameter of 10 nm) incubated with (E) RAW264.7 macrophage cells, (F) U87MG glioblastoma cells, (G) MDA-MB-231 breast cancer cells, (H) MCF-7 breast cancer cells at 37 °C for three hours at the Fe concentration of 0.2 mg/mL; and SHP-10 (with a core diameter of 10 nm) incubated with (I) RAW264.7 macrophage cells at the Fe concentration of 0.025 mg/mL, (J) U87MG glioblastoma cells, (K) MDA-MB-231 breast cancer cells, and (L) MCF-7 breast cancer cells at the Fe concentration of 0.2 mg/mL at 37 °C for three hours. Scale bar, 20  $\mu\text{m}$ .

*b*-AGE polymer coated IONP showed little change in hydrodynamic size in both PBS and 10% NaCl solution. When 0.9% NaCl solution was used to mimic the physiological ionic strength, PEG-*b*-AGE polymer coated IONP demonstrated good stability in 0.9% NaCl solution as well.

### Reduced non-specific cell uptake of nanoparticles and improved targeting

The innate immune system or the non-specific immune system, including monocytes, macrophages, dendritic cells, etc., is responsible for the immune response and cleaning out foreign materials from the body.<sup>59,60</sup> Macrophages in particular play the key role in clearance of nanoparticles and reducing the long term toxicity, recognizing and then engulfing systemically administered nanoparticles.<sup>61</sup> However, non-specific macrophage uptake of nanoparticles and ensuing migrations lead to shortened blood circulation and low level of delivery of nanoparticle probes to the targeted diseased region as well as off-target background signals.

In this work, RAW264.7 macrophage, a frequently used mouse macrophage cell line, was selected to examine the capability of PEG-*b*-AGE coated IONPs to avoid non-specific cellular uptake before and after conjugations with targeting ligands. Before the conjugation with targeting ligands, the PEG-*b*-AGE polymer coated IONP showed no uptake by macrophages after incubating with RAW264.7 cells for three hours at the Fe concentration of 0.2 mg/mL (**Figure 4A and 5A**). After the conjugation with ligands RGD or Tf, it was found that the RGD-conjugated PEG-*b*-AGE polymer coated IONPs (RGD-IONP) still showed no uptake by macrophages (**Figure 4E**), even though the surface property of the particle had been altered due to the introduction of the targeting ligands. **Figure 5E** shows that the macrophage cells exhibited a very low level uptake of Tf-conjugated PEG-*b*-AGE polymer coated IONP (Tf-IONP), which can be attributed to a low level expression of TfR in RAW264.7 macrophage. As a control, the amphiphilic polymer coated SHP-10 exhibited significant uptake by macrophages even at the Fe concentration of 0.025 mg/mL (**Figure 4I and 5I**).

The improved targeting capabilities as the result of the anti-biofouling property of the conjugated RGD or Tf conjugated PEG-*b*-AGE polymer coated IONPs were examined *in vitro* using different cancer cell lines with different cell marker expressions. For RGD-IONP, MDA-MB-231 breast cancer cells and U87MG glioblastoma cells were selected as the positive control for testing RGD targeting the tumor integrin because both cells have high expression of the integrin  $\alpha_v\beta_3$ .<sup>62,63</sup> MCF-7 breast cancer cells with low expression of the integrin  $\alpha_v\beta_3$  were used as the negative control.<sup>62</sup> As shown in **Figure 4**, before the conjugation of RGD targeting ligand, no PEG-*b*-AGE coated IONP uptake was observed for all three different cancer cell lines (**Figure 4B, C, and D**). After conjugating with RGD targeting ligands, only cells with high expression of the integrin  $\alpha_v\beta_3$ , i.e., U87MG and MDA-MB-231, exhibited the uptake of RGD-IONPs (**Figure 4F and G**), but not with the negative control MCF-7 breast cancer cells (**Figure 4H**). In comparison, an intensive uptake of amphiphilic copolymer coated SHP-10 by U87MG, MDA-MB-231, and MCF-7 cells was observed even without the conjugation of RGD targeting ligand (**Figure 4J, K, and L**), which suggested the attenuation of targeting efficiency as a result of the off-target effect and background interference from non-specific normal cell uptake. The cell uptake results and the comparison clearly demonstrated the excellent targeting specificity of the RGD conjugated PEG-*b*-AGE polymer coated IONP attributed to its anti-biofouling property to avoid non-specific cell uptake.

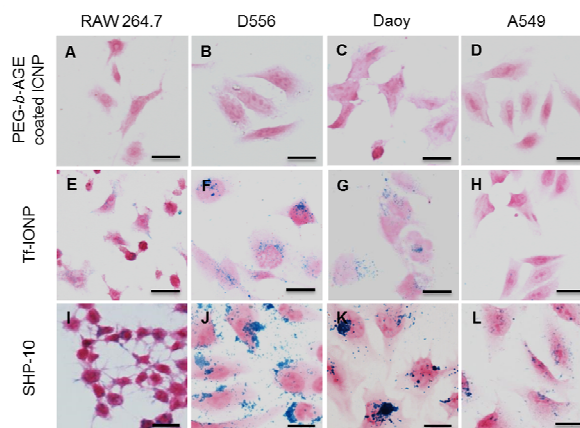


**Figure 5** Prussian blue stained images of PEG-*b*-AGE polymer coated IONP (with a core diameter of 10 nm) incubated with (A) RAW264.7 macrophage cells, (B) D556 medulloblastoma cells, (C) Daoy medulloblastoma cells, (D) A549 lung cancer cells; and Tf-IONP (with a core diameter of 10 nm) incubated with (E) RAW264.7 macrophage cells, (F) D556 medulloblastoma cells, (G) Daoy medulloblastoma cells, (H) A549 lung cancer cells at 37 °C for three hours at the Fe concentration of 0.2 mg/mL; and SHP-10 (with a core diameter of 10 nm) incubated with (I) RAW264.7 macrophage cells at the Fe concentration of 0.025 mg/mL, (J) D556 medulloblastoma cells, (K) Daoy medulloblastoma cells, and (L) A549 lung cancer cells at the Fe concentration of 0.2 mg/mL at 37 °C for three hours. Scale bar,

For testing Tf-IONP, D556 and Daoy medulloblastoma cells with high expression of TfR were selected for the experiments. Lung cancer A549 cells with very low levels of TfR expression were used as a control. As shown in **Figure 5**, no uptake of PEG-*b*-AGE coated IONPs was observed for all three different cancer cells (**Figure 5B, C, and D**). However, when using Tf-IONPs, only the D556 and Daoy cancer cells with high expression of the TfR exhibited the uptake of the Tf-IONPs (**Figure 5F and G**), but no uptake of Tf-IONP could be observed for the control of A549 lung cancer cells (**Figure 5H**). In contrast, intensive uptake of the non-targeted SHP by D556, Daoy and A549 cells was observed, making it difficult to differentiate the different levels of TfR in different cells. Taken together, the results clearly indicated the excellent and improved targeting specificity and efficiency of the ligand conjugated PEG-*b*-AGE polymer coated IONP by minimizing non-specific cell uptake with anti-biofouling properties.

### *In vitro* cell cytotoxicity analysis

In order to apply the PEG-*b*-AGE polymer coated IONP to biomedical purposes, a cytotoxicity evaluation of the particle was carried out. RAW264.7 macrophage cells, U87MG glioblastoma cells, MDA-MB-231 breast cancer cells, MCF-7 breast cancer cells, Hela cells, D556 medulloblastoma cells, Daoy medulloblastoma cells, and A549 lung cancer cells were selected to incubate with PEG-*b*-AGE coated IONP (with a core diameter of 10 nm) with Fe concentration ranging from 0.500 mg/mL to 0.008 mg/mL for 24 hours. Afterwards, cell viability was estimated using the MTT conversion test. As shown in **Figure 6**, even when the PEG-*b*-AGE polymer coated IONP was added at exceedingly high concentrations at 0.500 mg/mL, the cell survival rates still reached 83% for macrophage cells. The PEG-*b*-AGE polymer coated IONP at lower concentrations did not exhibit statistically significant cytotoxicity ( $p \geq 0.05$ ). For cancer cells, cell viabilities started to decrease when

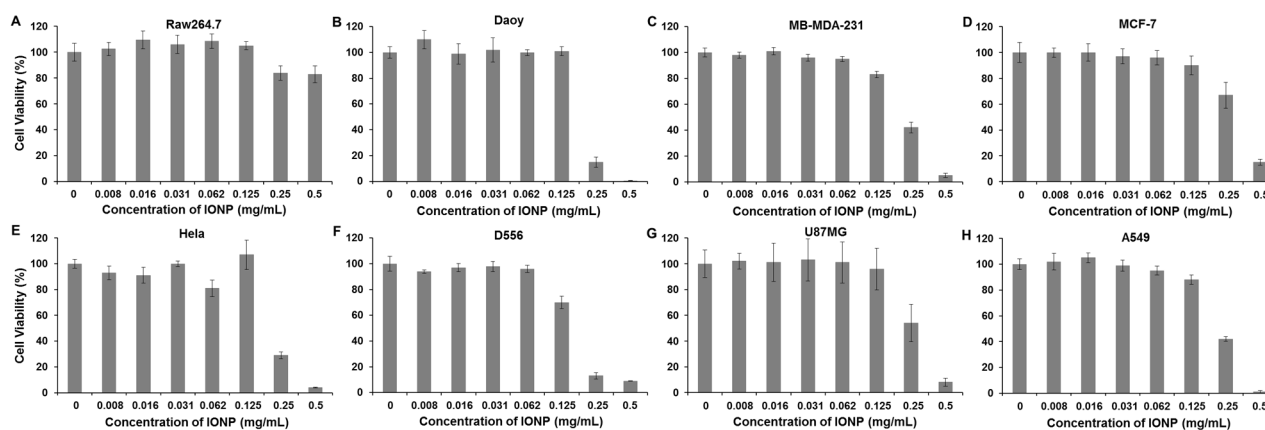


**Figure 6.** Cell viabilities of PEG-*b*-AGE polymer coated IONPs in: (A) RAW264.7 macrophages, (B) Daoy medulloblastoma cells, (C) MB-MDA-231 breast cancer cells, (D) MCF-7 breast cancer cells, (E) HeLa cells, (F) D556 medulloblastoma cells, (G) U87MG glioblastoma cells, and (H) A549 lung cancer cells. MTT assays were performed by treating cells with PEG-*b*-AGE polymer coated IONPs for 24 hours

treated with PEG-*b*-AGE polymer coated IONPs at higher concentrations (0.250 and 0.500 mg/mL). The patterns of reduced cell viabilities were also observed when treating these cells with PEG-*b*-AGE polymer coated IONPs for much longer time (3 days) (shown in Supporting Information). The MTT assays were also performed for RGD conjugated and Tf conjugated IONPs using the same cell lines, the results of cell viabilities can be found in Supporting Information.

### Target specific MRI contrast change and reduction of off-target background

IONPs are mostly used as superb  $T_2$ -weighted MRI contrast agents, typically causing signal drops in MRI<sup>29,30</sup> by sharply shortening the transverse relaxation time  $T_2$  and dephasing the signal with induced susceptibility.<sup>64</sup> To assess the potential of the PEG-*b*-AGE polymer coated IONP being an imaging probe, the transverse relaxation time  $T_2$  was determined by fitting the MRI signal intensities at different echo times ( $n = 20$ ) with an exponential function. The transverse relaxivity ( $r_2$ ) was calculated from the slopes of the linear correlation between the relaxation rates ( $1/T_2$ ) and iron concentrations. A typical hypointense contrast from the PEG-*b*-AGE polymer coated IONP was observed in  $T_2$ -weighted spin echo images (Figure 7A), and the transverse relaxivities of the IONPs were calculated to be  $57.6 \text{ mM}^{-1} \text{ s}^{-1}$  and  $162.6 \text{ mM}^{-1} \text{ s}^{-1}$  respectively for nanoparticles with core diameters of 10 nm and 20 nm (Figure 7B).

To examine whether reducing non-specific uptake and off-target

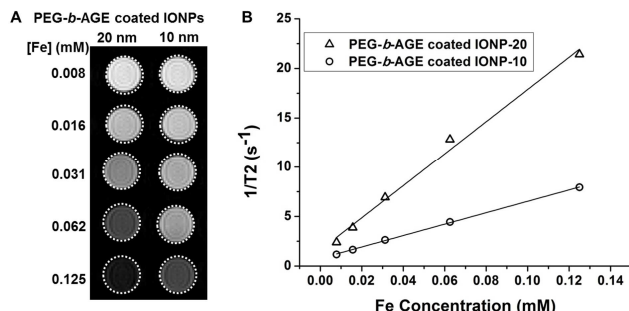


**Figure 7.** (A)  $T_2$ -weighted spin echo MR images of PEG-*b*-AGE coated IONPs (with core diameters of 10 and 20 nm) at different concentrations; and (B) transverse relaxation rates ( $R_2$  or  $1/T_2$ ,  $\text{s}^{-1}$ ) of PEG-*b*-AGE coated IONPs (with core diameters of 10 and 20 nm) as a function of the Fe concentration (mM).

background by anti-biofouling PEG-*b*-AGE polymer can improve specificity of MRI contrast change that is directly related to the targeting cell biomarker, we prepare the cell phantoms containing D556 medulloblastoma cells, A549 lung cancer cells, and RAW264.7 macrophage cells, treated with Tf conjugated IONPs with or without anti-biofouling PEG-*b*-AGE coating. Because 20 nm particle has greater transverse relaxation rate ( $R_2$ ) than 10 nm particle (i.e. better contrast under same condition), the PEG-*b*-AGE coated IONP with a core diameter of 20 nm and SHP-20 were used for the phantom preparation.  $R_2$  (or  $1/T_2$ ) relaxometry mapping of these cell phantoms showed substantial increase of  $R_2$  values in cells (e.g., D556, A549 and RAW264.7 cells) treated with SHP-20 but no significant change of  $R_2$  value in cells treated with PEG-*b*-AGE polymer coated IONPs, with the exception of a slight increase of the  $R_2$  values in PEG-*b*-AGE polymer coated IONPs with D556 medulloblastoma cancer cells (Figure 8A and C). Since  $R_2$  value is directly proportional to the amount of IONP taken up by cells (i.e. the higher the  $R_2$  value, the more IONP taken up by cells), the  $R_2$  (or  $1/T_2$ ) relaxometry results from cell phantom (in Figure 8A and C) suggest a significant reduction of off-target background with PEG-*b*-AGE polymer coated IONPs comparing to conventional polymer coated SHP-20, attributed to the anti-biofouling effect of the PEG-*b*-AGE coating polymer. With transferrin as the targeting ligand, Both Tf-SHP and PEG-*b*-AGE polymer coated Tf-IONP showed expected increase of contrast or “darkening” in  $T_2$ -weighted MRI (increased  $R_2$  value) in D556 cells compared to non-targeted SHP-20 and IONPs as well as the control A549 cells (Figure 8B and D), due to a higher level of transferrin receptor expression in D556 cells. However, The control A549 cells treated with TfR targeted SHP-20 showed substantially lower signal level comparing to A549 cells treated with PEG-*b*-AGE polymer coated Tf-IONP, suggesting that anti-biofouling effect from PEG-*b*-AGE polymer coated Tf-IONP led to the reduction of non-specific uptake of targeted IONPs by the cells not presenting targeted biomarkers, therefore, attenuated off-targeted background signal (Figure 8B and D). Taking together, receptor targeted PEG-*b*-AGE polymer coated IONPs can improve targeted specific delivery and image contrast by not only maintaining ligand-target interactions without interference of “protein corona” or other surface adhesion of biomolecules, but also reducing the off-target background signals led by non-specific cell uptake of targeted IONPs. The reduction of the background from the non-specific off-targeting signal is important, as this improvement allows for considering using targeted nanoparticle imaging probes (e.g., MRI, optical imaging or nuclear imaging) to determine and even quantify the levels of targeted biomarkers. The imaging probes

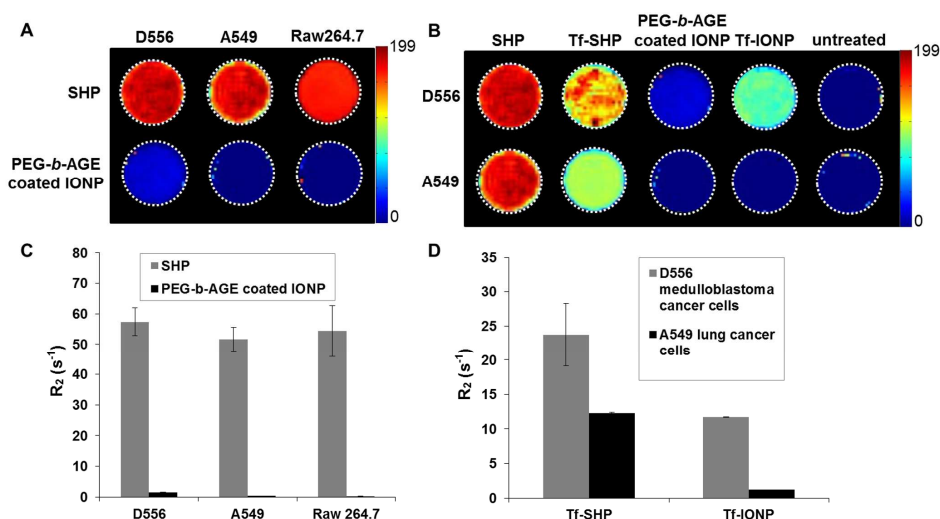


**Figure 8.**  $R_2$  relaxometry maps of (A) cell phantoms containing  $8 \times 10^6$  D556 medulloblastoma cells, A549 lung cancer cells, and RAW264.7 macrophage cells showed different levels of  $R_2$  value change after incubation with SHP-20 and PEG-*b*-AGE coated IONP (with a core diameter of 20 nm); and (B) cell phantoms containing  $8 \times 10^6$  D556 medulloblastoma cells and A549 lung cancer cells treated with SHP-20, TfR targeted SHP-20 (Tf-SHP), PEG-*b*-AGE coated IONP, and TfR targeted PEG-*b*-AGE coated IONP (Tf-IONP). The differences in  $R_2$  values indicate improved targeting by the anti-biofouling property of PEG-*b*-AGE coated IONP.  $R_2$  values of cell phantoms containing (C) D556 medulloblastoma cells, A549 lung cancer cells, and RAW264.7 macrophage cells treated with SHP and PEG-*b*-AGE coated IONP, and (D) D556 medulloblastoma cells and A549 lung cancer cells treated with Tf-SHP, and Tf-IONP. Signal intensities are normalized by subtracting the signal intensities of the cells incubated with regular media without nanoparticles.

thus not only can detect the overexpressed disease biomarkers, but also provide the quantitative capability to monitor disease progression or treatment responses. Furthermore, the reduction of off-target uptake of nanoparticles in background may also benefit the nanoparticle based drug delivery by improving the targeted delivery and minimizing the toxicity due to the normal tissue uptake.

## Experimental

### Materials

Sodium hydride (dry, 95%), sodium sulfate (anhydrous), sodium hydroxide (97%), nickel perchlorate hexahydrate, pyrocatechol violet, methanesulfonyl chloride (99.5%), sodium azide (99%), triphenylphosphine (99%), poly (ethylene glycol) (PEG) 1000 (Molecular weight = 1000 g/mol), allyl glycidyl ether (99%), 2,2-azobis(isobutyronitrile) (AIBN, 98%), (3-mercaptopropyl)trimethoxysilane (95%), (3-aminopropyl)trimethoxysilane (97%), ninhydrin, sodium acetate trihydrate, 1,10-phenanthroline (99%), ethanol (200 proof), deionized water, dichloromethane (ACS grade), and toluene (anhydrous) were purchased from Sigma-Aldrich and used as received. Tetrahydrofuran (THF) was purchased from Sigma-Aldrich, and dried by distillation over sodium before use. Triethylamine (99.5%) was purchased from Sigma-Aldrich, and dried by 3 Å molecular sieves. Agarose was purchased from Fisher. Oleic acid coated IONPs (with an averaged core diameter of 10 nm or 20 nm), amphiphilic polymer coated water-soluble IONP (SHP), activation buffer (pH 5.5), and coupling buffer (pH 8.5) were obtained from Ocean Nanotech LLC. Sulfo-succinimidyl-4-(N-maleimidomethyl)cyclohexane-1-carboxylate (Sulfo-SMCC), 2-Imino-thiolane•HCl (Traut's reagent), N-(hydroxysulfosuccinimide) (Sulfo-NHS), 1-ethyl-3-[3-dimethylaminopropyl]carbodiimide hydrochloride (EDC), and BCA protein assay kit were purchased from Thermo Scientific.

MTT assay kit was purchased from Sigma-Aldrich. Peptide cyclo-(RGDFC) (RGD) was purchased from Bachem. Holo-transferrin (human) was purchased from Sigma-Aldrich. The main text of the article should go here with headings as appropriate.

### Synthesis of NH<sub>2</sub>-PEG (1)

As shown in **Scheme 1**, PEG 1000 (4.0 g, 4 mmol, dried by vacuum at 40 °C for 3 hours) was dissolved in distilled THF (50 mL) under argon atmosphere. The solution was cooled to 0 °C using an ice/water bath, before methanesulfonyl chloride (0.50 mL, 6.0 mmol) was added by syringe. Triethylamine (1.25 mL, 9.0 mmol) was then slowly introduced by syringe with immediate formation of a white precipitate. The mixture was allowed to warm to room temperature and stirred overnight under argon. The reaction contents were concentrated and dissolved in ethanol (75 mL). Sodium azide (2.60 g, 40.0 mmol) was then added to the solution, and the reaction was heated to reflux for 18 hours. After cooling, the solvent was removed under reduced pressure. The residue was dissolved with deionized water, transferred to a separatory funnel, and extracted with DCM three times. The combined organic layers were dried over anhydrous Na<sub>2</sub>SO<sub>4</sub>, filtered, and concentrated by rotary evaporator. The residue was dissolved in THF (100 mL), and deionized water (20 mL) was added along with triphenylphosphine (5.33 g, 20 mmol). The reaction was stirred at room temperature overnight. The reaction contents were then concentrated, dissolved in a 0.1 M NaOH aqueous solution, and transferred to a separatory funnel. The solution was washed with a diethyl ether/hexane (80/20) solution, and then extracted with DCM three times. The combined organic layers were dried over anhydrous Na<sub>2</sub>SO<sub>4</sub>, then filtered, and concentrated. The residue was recrystallized from ethyl acetate/hexane to yield white waxy solid (77.5% yield). <sup>1</sup>H NMR (CDCl<sub>3</sub>) δ 3.70 - 3.54 (complex m, 84 H), 2.89 (br s, 1 H), 2.50 (br, s, 2 H) ppm; <sup>13</sup>C NMR δ 74.12, 72.68, 70.79, 70.74, 70.53, 61.88,

42.44 ppm. MALDI peak mass ( $m/z$ ) found: 920 g/mol ( $n = 20 + \text{Na}$ ).

### Synthesis of $\text{NH}_2$ -PEG-AGE (2)

$\text{NH}_2$ -PEG **1** (1g, 1 mmol) was dissolved in toluene (30 mL) under argon atmosphere. NaH (36 mg, 1.5 mmol) was then added to the solution. The reaction was heated to 60 °C for 1 hour. Allyl glycidyl ether (0.15 mL, 1.1 mmol) was introduced by syringe to the solution. The reaction was heated up to reflux for 12 hours. The reaction contents were concentrated. The residue was dissolved in the minimal amount of isopropyl alcohol, transferred to a centrifuge tube, and precipitated by addition of cold diethyl ether (-20 °C). The mixture was kept in -20 °C freezer overnight. The mixture was centrifuged, and the supernatant was decanted. The precipitation was repeated twice more, and the solid residue was lyophilized to yield brown solid (94% yield).  $^1\text{H}$  NMR ( $\text{CDCl}_3$ )  $\delta$  5.91 - 5.80 (m, 1 H), 5.22 (d, 1 H), 2.12 (d, 1 H), 3.95 (d, 2 H), 3.74 - 3.42 (complex m, 88 H) ppm.  $^{13}\text{C}$  NMR  $\delta$  134.86, 117.34, 74.03, 72.58, 70.71, 70.70, 70.48, 42.26 ppm. MALDI peak mass ( $m/z$ ) found: 1034 g/mol ( $n = 20 + \text{Na}$ ).

### Synthesis of diblock copolymer PEG-*b*-AGE (3)

The flask containing  $\text{NH}_2$ -PEG-AGE **2** (0.22 g, 0.2 mmol), AIBN (11 mg, 0.066 mmol), and (3-mercaptopropyl) trimethoxysilane (0.40 mL, 2 mmol) was degassed for 15 min by vacuum, and then distilled THF (20 mL) was added by syringe under argon atmosphere. The reaction was heated up to 70 °C for 24 hours. The reaction contents were then concentrated and the residue was washed by hexane for several times to remove the unreacted (3-mercaptopropyl) trimethoxysilane. The washed residue was dried under vacuum to yield light-yellow solid (81% yield).  $^1\text{H}$  NMR ( $\text{CDCl}_3$ )  $\delta$  3.70 - 3.38 (complex m, 104 H), 2.58 - 2.50 (m, 4 H), 1.84 (m, 2 H), 1.69 (m, 2 H), 0.75 (t, 2 H) ppm.  $^{13}\text{C}$  NMR  $\delta$  72.40, 71.04, 70.44, 43.01, 35.48, 32.06, 30.26, 29.07, 28.08, 14.61, 9.09 ppm.

### Coating and stabilizing IONPs with diblock polymer PEG-*b*-AGE

PEG-*b*-AGE copolymer was then applied to coat hydrophobic IONPs in the organic solvent based on **Scheme 2**. Oleic acid coated IONPs (10 mg, with a core diameter of 10 nm or 20 nm) were dispersed in THF (2 mL). The IONP THF solution was added to the PEG-*b*-AGE solution in THF (18 mL, 5 mg/mL), and stirred for 24 hours at room temperature, allowing for exchange of oleic acids on the IONP surface with PEG-*b*-AGE polymers. The mixture was then added dropwise to deionized water (200 mL). The resultant solution was dialyzed against water for 48 hours to remove THF and unreacted polymer. The aqueous solution was then centrifuged at

3000 rpm for 5 min to eliminate any large aggregates, yielding the PEG-*b*-AGE coated IONP final product.

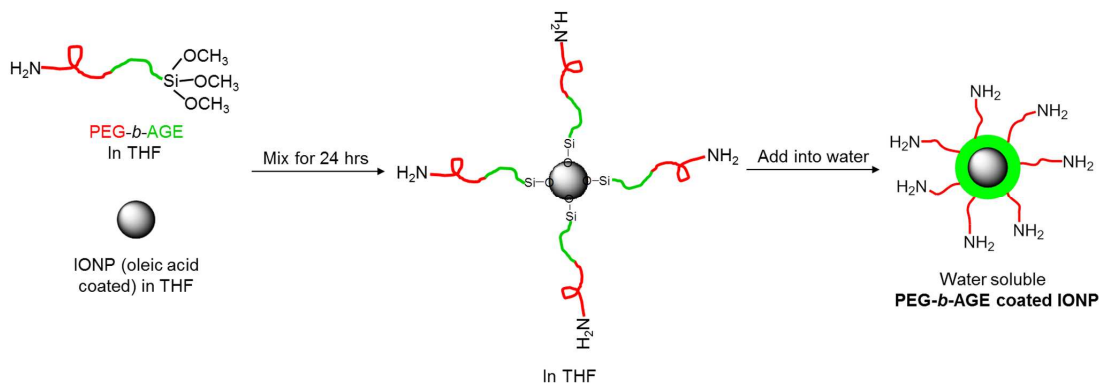
### Characterization of PEG-*b*-AGE coating polymer and the PEG-*b*-AGE coated IONP

The PEG-*b*-AGE coating polymer was characterized by nuclear magnetic resonance (NMR) instrument (Varian INOVA 400 spectrometer) using  $\text{CDCl}_3$  as solvent, and matrix-assisted laser desorption/ionization (MALDI) spectrometry (Applied Biosystems Voyager-DE) using 2,5-dihydroxybenzoic acid matrix.

The average hydrodynamic diameters and the  $\zeta$ -potential of the PEG-*b*-AGE coated IONPs were measured by dynamic light scattering (DLS) instrument (Malven Zeta Sizer Nano S-90) equipped with a 22 mW He-Ne laser operating at  $\lambda = 632.8$  nm. The core diameters of IONP and the thickness of coating polymer layers were viewed and measured using transmission electron microscopy (TEM) (Hitachi H-7500 instrument (75 kV)). A drop of diluted solution was put on the grid and dried in the air.

The concentration of PEG-*b*-AGE coated IONP was determined using the 1,10-phenanthroline colorimetric method.<sup>64</sup> Then the IONP concentration was calculated based on the assumption that the nanoparticle was spherical with a bulk magnetite density of 5.18  $\text{g}/\text{cm}^3$ .

The number of  $-\text{NH}_2$  groups introduced on the PEG-*b*-AGE coated IONP was quantified using ninhydrin.<sup>65-67</sup> Briefly, the ninhydrin stock solution was made by dissolving ninhydrin (1.2 mmol, 213.8 mg) and sodium acetate trihydrate (12.0 mmol, 1632.0 mg) in ethanol (6 mL) and DI  $\text{H}_2\text{O}$  (6 mL). (3-aminopropyl)trimethoxysilane was used to make a standard curve plotted of the concentration of  $-\text{NH}_2$  groups in mM ( $Y$ ) versus the absorbance of the product derived from ninhydrin and  $-\text{NH}_2$  group at 570 nm ( $X$ ). The (3-aminopropyl)trimethoxysilane in ethanol solution was prepared and the concentration ranged from 1  $\mu\text{M}$  to 5 mM. 500  $\mu\text{L}$  of the ninhydrin stock solution was mixed with 200  $\mu\text{L}$  of the (3-aminopropyl)trimethoxysilane solution at different concentrations, and heated to 80 °C for 15 min as the solution turns purple color (Ruhemann's purple). After the solutions were cooled to the room temperature, the absorbance at 570 nm was recorded from 200  $\mu\text{L}$  of the solution from each sample to plot the standard curve. To quantify the number of  $-\text{NH}_2$  groups on the PEG-*b*-AGE coated IONP, 200  $\mu\text{L}$  of the PEG-*b*-AGE coated IONP with a known concentration was mixed with 500  $\mu\text{L}$  of the ninhydrin stock solution and 1 M sodium acetate solution in ethanol/ $\text{H}_2\text{O}$  (50/50). Both solutions were heated to 80 °C for 15 min. After being cooled down to the room temperature, 200  $\mu\text{L}$  of the solution from each sample was taken to measure the absorbance at 570 nm. The number of  $-\text{NH}_2$  groups on the surface of PEG-*b*-AGE coated IONP ( $N$ ) was then determined using the equation (1), where  $X_1$  and  $X_2$  are the



**Scheme 2.** Schematic illustration of the preparation of water soluble PEG-*b*-AGE coated IONP.

absorbance of PEG-*b*-AGE coated IONP with ninhydrin stock solution and sodium acetate solution, respectively;  $K_1$  is the slope derived from the standard curve,  $c$  is the constant derived from the standard curve, and  $C_{\text{IONP}}$  is the concentration of PEG-*b*-AGE coated IONP in the unit of mM.

$$N = \frac{K_1 (X_1 - X_2) + c}{C_{\text{IONP}}} \quad (1)$$

The transverse relaxation times ( $T_2$ ) and relaxivity ( $r_2$ ) of IONPs were determined using a 3 Tesla MR scanner (Tim/Trio, Siemens, Erlangen, Germany). Solutions of PEG-*b*-AGE coated IONPs (with a core diameter of 10 nm or 20 nm) with different iron concentrations ranging from 0.0045 to 0.0700 mM were prepared and imaged with a multi-echo spin echo (SE) sequence using TR of 2520 ms and 20 TEs, starting at 12.2 ms with increments of 12.2 ms. Mean signal intensity values from regions of interest (ROI) selected from the images of each sample were measured and calculated using ImageJ (National Institutes of Health, Bethesda, MD, USA). The value of the  $T_2$  relaxation time was calculated from the measured average signal intensity ( $I$ ) at different TEs using a non-linear exponential curve fitting based on Equation (2).

$$I = K_2 e^{-TE/T_2} \quad (2)$$

#### Examination of stability of PEG-*b*-AGE coated IONP

The stability of the PEG-*b*-AGE coated IONP was evaluated by measuring the average hydrodynamic diameters of the nanoparticles in phosphate buffered saline (PBS), 10% (w/v) NaCl aqueous solution, 0.9% (w/v) NaCl aqueous solution, and 100% fetal bovine serum (FBS) at the concentration of 0.1 mg/mL at 1, 2, 4, 8, 12, and 24 hours, respectively. The 10% (w/v) NaCl aqueous solution was used to demonstrate the stability of the PEG-*b*-AGE coated IONP under great ionic strength. 0.9% (w/v) NaCl solution (saline solution) was utilized to mimic the physiological environment. One hundred percent FBS solution contains a high concentration of proteins, thus was used for testing whether PEG-*b*-AGE coated IONP is stable upon exposure to proteins in the media. The hydrodynamic diameter change of nanoparticles in FBS would be a direct indication of the formation of a protein corona and possible aggregation as a result. A commercially available amphiphilic polymer coated water-soluble IONP (SHP-20) obtained from Ocean NanoTech was used as the control for comparison. The hydrodynamic diameter change of the SHP-20 (with a core diameter of 20 nm) was also measured in 10% FBS at the concentration of 0.1 mg/mL at 1, 2, 4, 8, 12, and 24 hours, respectively.

#### Measurement of surface adsorption of proteins

To investigate the formation of the protein corona on the surface of IONPs, PEG-*b*-AGE coated IONP (with a core diameter of 20 nm, 0.25 mg) and SHP (with a core diameter of 20 nm, 0.25 mg) were incubated with 100% FBS (2 mL) and human plasma (2 mL) for one hour at 37 °C, since a stable protein corona will form over a period of one hour.<sup>51,52</sup> IONPs were then separated from the media using a magnetic separator. The resultant IONPs were washed with PBS (1 mL) to remove the unattached free proteins, and followed by magnetic separation. The wash-separation process was repeated three times. After free proteins were removed, IONPs were then further washed with 0.1 M KCl solution (1 mL) to wash off the proteins attached to the surface.<sup>50</sup> After IONPs were removed from the KCl solution by a magnetic separator, the amount of proteins in

the KCl solution was quantified using the bicinchoninic acid (BCA) protein assay.<sup>68</sup>

#### Quantification of the number of -COOH group on surface

The amount of COOH group on surface was determined using a colorimetric method via the simultaneous binding between  $\text{Ni}^{2+}$  and COOH.<sup>69</sup> Briefly,  $\text{Ni}(\text{ClO}_4)_2$  was added to 100  $\mu\text{L}$  of the IONP solution in PBS to make the final  $\text{Ni}^{2+}$  concentration of 200  $\mu\text{M}$ . After incubating for 10 min, the solution was filtered to remove the IONP. Pyrocatechol violet was then added to the resultant solution to make the final concentration of 200  $\mu\text{M}$ . The absorbance at 650 nm was measured to determine the free  $\text{Ni}^{2+}$  left in the solution. The standard curve of absorbance at 650 nm was plotted against the concentrations of acetic acid (0.8  $\mu\text{M}$  to 1 mM). The COOH concentration (mM) in the original IONP solution can be derived from the concentration difference between added and detected  $\text{Ni}^{2+}$  ion. The average number of COOH group on surface is quantified by dividing the COOH concentration (mM) by the concentration of IONP (mM).

#### Conjugation of the small RGD peptide

As shown in **Scheme 3**, the PBS solution of PEG-*b*-AGE coated IONP (concentration of 2 mg/mL) was incubated with the linker sulfo-succinimidyl-4-(*N*-maleimidomethyl)cyclohexane-1-carboxylate (Sulfo-SMCC, at the concentration of 2 mg/mL) for one hour. The solution was purified with a PD-10 column pre-saturated with PBS, followed by incubation with tumor targeting peptide, cyclo-(Arg-Gly-Asp-D-Phe-Cys) or (RGD), at the concentration of 0.2 mg/mL for one hour. The solution of RGD conjugated IONP (RGD-IONP) was obtained after purification with a PD-10 column pre-saturated with PBS. The average number of RGD conjugated to IONP is derived by comparing the RGD concentration (equals to COOH concentration) with the IONP concentration in the RGD-IONP solution.

#### Conjugation of the large protein transferrin (Tf)

As shown in **Scheme 3**, the PEG-*b*-AGE coated IONP was made solution in PBS at the concentration of 2 mg/mL, which was then incubated with the linker Sulfo-SMCC (at the concentration of 2 mg/mL) for one hour. After incubation, the solution was purified with a PD-10 column pre-saturated with PBS to remove the impurity produced during the incubation, obtaining the SMCC modified IONP (SMCC-IONP). On the other hand, transferrin (Tf) was mixed with Traut's Reagent (in the molar ratio of 1:15) in 0.1 M borate buffer (pH 8.5). The solution was incubated overnight at room temperature protected from light. The excess Traut's reagent was removed using a desalting spin column to obtain the thiolated transferrin (Tf-SH). The SMCC-IONP and Tf-SH were then mixed in PBS, and incubated at room temperature for four hours. The transferrin conjugated IONP (Tf-IONP) was separated from the solution using magnetic separator, and washed with PBS. The separation-wash process was repeated three times at 4 °C. The amount of transferrin conjugated to the IONP was derived by comparing the protein concentration of the Tf-IONP, measured by BCA protein assay, with the IONP concentration of the Tf-IONP, determined using the 1,10-phenanthroline colorimetric method.

To make a control sample for testing cell targeting efficiency and targeted imaging, conventional amphiphilic triblock polymer coated SHP-20 was used for conjugating Tf using a protocol published previously,<sup>64</sup> briefly, sulfo-NHS and EDC were added to 1 mg of SHP-20 (0.2 mL, 5 mg/mL) mixed with 0.1 mL activation buffer (pH 5.5) to form final concentrations of 0.125 mg/mL and 0.25 mg/mL respectively. The solution was centrifuged with Centrifugal Devices (MWCO: 300 K, Nanosep) at 2500 rpm for 10 min to



DMSO with pipetting for 5 min. Absorbance at 570 nm was measured on a plate reader. Readings from 6 wells were averaged, and 100% viability was determined for untreated cells. Comparisons of the cell viability with different Fe concentrations with control were performed using one-way analysis of variance and the student *t* test (unpaired, two tails).

## Conclusions

A novel diblock copolymer PEG-*b*-AGE with capabilities of facile conjugation with different targeting ligands and reducing non-specific protein adsorption and cell uptake has been developed to coat and stabilize IONP. This coating polymer demonstrated an excellent anti-biofouling effect to prevent the formation of protein corona and the non-specific uptake by a variety of human cancer cell lines. As a consequence of the excellent anti-biofouling property, surface functionalized PEG-*b*-AGE coated IONP conjugated with targeting ligands showed significantly improved targeting specificity and efficiency by reducing off-target and non-specific interactions with biological media, which should enable highly specific targeted drug delivery and imaging with nanoparticles.

## Acknowledgements

This work is supported in parts by NIH R01CA154846-02 (HM and YL), NCI's Cancer Nanotechnology Platform Project (CNPP) grant U01CA151810-02 (HM and YL), and a seed grant from the Center for Pediatric Nanomedicine of Children's Healthcare of Atlanta (HM and TM).

## Notes and references

<sup>a</sup> Department of Radiology and Imaging Sciences, Emory University School of Medicine, Atlanta, GA 30322, USA

<sup>b</sup> Department of Radiology, the First Affiliated Hospital of Sun Yat-Sen University, Guangzhou, Guangdong, China

<sup>c</sup> Department of Radiology, Nanjing University College of Medicine and Affiliated Drum Tower Hospital, Nanjing, Jiangsu, China

<sup>c</sup> Department of Pediatrics, Emory University School of Medicine, Atlanta, GA 30322, USA

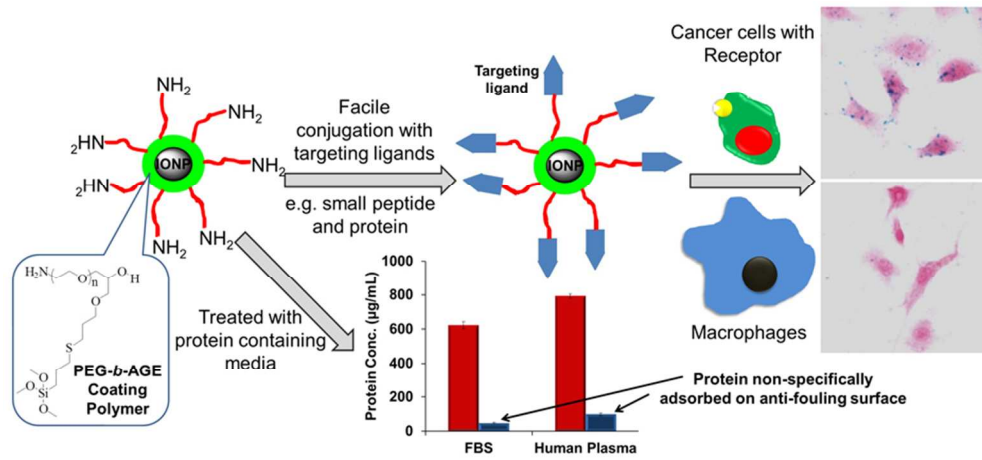
<sup>e</sup> Department of Surgery, Emory University School of Medicine, Atlanta, GA 30322, USA

† These authors contribute equally.

- 1 A. Z. Wang, R. Langer and O. C. Farokhzad, *Annu. Rev. Med.* 2012, **63**, 185.
- 2 Y. Liu and M. J. Welch, *Bioconjugate Chem.* 2012, **23**, 671.
- 3 W. R. Sanhai, J. H. Sakamoto, R. Canady and M. Ferrari, *Nat. Nanotechnol.* 2008, **3**, 242.
- 4 K. Riehemann, S. W. Schneider, T. A. Luger, B. Godin, M. Ferrari and H. Fuchs, *Angew. Chem. Intl. Ed.* 2009, **48**, 872.
- 5 S. Nie, Y. Xing, G. J. Kim and J. W. Simons, *Ann. Rev. Biomed. Eng.* 2007, **9**, 257.
- 6 J. R. Heath and M. E. Davis, *Annu. Rev. Med.* 2008, **59**, 251.
- 7 M. Elsbahy and K. L. Wooley, *Chem. Soc. Rev.* 2012, **41**, 2545.
- 8 S. Nie, *Nanomedicine* 2010, **5**, 523.
- 9 B. D. Ratner, A. S. Hoffman, F. J. Schoen and J. E. Lemons, *Biomaterials science, an introduction to materials in medicine. 2nd Ed.*; Elsevier: Amsterdam, 2004.
- 10 R. Langer, *Science* 2001, **293**, 58.
- 11 C. C. Berry and A. S. G. Curtis, *J. Phys. D Appl. Phys.* 2003, **36**, R198.

- 12 N. L. Anderson, M. Polanski, R. Pieper, T. Gatlin, R. S. Tirumalai, T. P. Conrads, T. D. Veenstra, J. N. Adkins, J. G. Pounds, R. Fagan and A. Lobley, *Mol. Cell. Proteomics* 2004, **3**, 311.
- 13 T. Cedervall, I. Lynch, S. Lindman, T. Berggard, E. Thulin, H. Nilsson, K. A. Dawson and S. Linse, *Proc. Natl. Acad. Sci.* 2007, **104**, 2050.
- 14 E. Casals, T. Pfaller, A. Duschl, G. J. Oostingh and V. Puntès, *ACS Nano*, 2010, **4**, 3623.
- 15 A. E. Nel, L. Madler, D. Velegol, T. Xia, E. M. V. Hoek, P. Somasundaran, F. Klaessig, V. Castranova and M. Thompson, *Nat. Mater.* 2009, **8**, 543.
- 16 D. E. I. Owens and N. A. Peppas, *Int. J. Pharm.* 2006, **307**, 93.
- 17 Z. J. Deng, M. Liang, M. Monteiro, I. Toth and R. F. Minchin, *Nat. Nanotechnol.* 2011, **6**, 39.
- 18 D. A. Hume, *Curr. Opin. Immunol.* 2006, **18**, 49.
- 19 L. Brannon-Peppas and J. O. Blanchette, *Adv. Drug Del. Rev.* 2004, **56**, 1649.
- 20 A. Salvati, A. S. Pitek, M. P. Monopoli, K. Prapainop, F. B. Bombelli, D. R. Hristov, P. M. Kelly, C. Aberg, E. Mahon and K. A. Dawson, *Nat. Nanotechnol.* 2013, **8**, 137.
- 21 A. Li, H. P. Leuhmann, G. Sun, S. Samarajeewa, J. Zou, S. Zhang, F. Zhang, M. J. Welch, Y. Liu and K. L. Wooley, *Acs Nano* 2012, **6**, 8970.
- 22 Y. Ji, Y. Wei, X. Liu, J. Wang, K. Ren and J. Ji, *J. Biomed. Mater. Res. A* 2012, **100A**, 1387.
- 23 L. Zhang, Z. Cao, T. Bai, L. Carr, J. R. Ella-Menye, C. Irvin, B. D. Ratner and S. Jiang, *Nat. Biotechnol.* 2013, **31**, 553.
- 24 H. Wei, N. Insin, J. Lee, H. S. Han, J. M. Cordero, W. Liu and M. G. Bawendi, *Nano Lett.* 2012, **12**, 22.
- 25 S. Zhang, J. Zou, F. Zhang, M. Elsbahy, S. E. Felder, J. Zhu, D. J. Pochan and K. L. Wooley, *J. Am. Chem. Soc.* 2012, **134**, 18467.
- 26 L. H. Reddy, J. L. Arias, J. Nicolas and P. Couvreur, *Chem. Rev.* 2012, **112**, 5818.
- 27 L. E. V. Vlerken, T. K. Vyas and M. M. Amiji, *Pharm. Res.* 2007, **24**, 1405.
- 28 Y. Sheng, C. Liu, Y. Yuan, X. Tao, F. Yang, X. Shan, H. Zhou and F. Xu, *Biomaterials* 2009, **30**, 2340.
- 29 H. Chen, X. Wu, H. Duan, Y. A. Wang, L. Wang, M. Zhang and H. Mao, *ACS Appl. Mater. Interfaces* 2009, **1**, 2134.
- 30 H. Chen, L. Wang, J. Yeh, X. Wu, Z. Cao, Y. A. Wang, M. Zhang, L. Yang and H. Mao, *Biomaterials* 2010, **31**, 5397.
- 31 H. Chen, L. Wang, Q. Yu, W. Qian, D. Tiwari, H. Yi, Y. A. Wang, J. Huang, L. Yang and H. Mao, *Int. J. Nanomedicine* 2013, **8**, 3781.
- 32 S. I. Jeon, J. H. Lee, J. D. Andrade and P. G. D. Gennes, *J. Colloid Interface Sci.* 1991, **142**, 149.
- 33 J. Satulovsky, M. A. Carignano and I. Szleifer, *Proc. Natl. Acad. Sci.* 2000, **97**, 9037.
- 34 I. Szleifer, *Biophys. J.* 1997, **72**, 595.
- 35 W. W. Yu, E. Chang, J. C. Falkner, J. Zhang, A. M. Al-Somali, C. M. Sayes, J. Johns, R. Drezek and V. L. Colvin, *J. Am. Chem. Soc.* 2007, **129**, 2871.
- 36 H. Duan, M. Kuang, X. Wang, Y. A. Wang, H. Mao and S. Nie, *J. Phys. Chem. C* 2008, **112**, 8127.
- 37 X. Gao, Y. Cui, R. M. Levenson, L. W. K. Chung and S. Nie, *Nat. Biotechnol.* 2004, **22**, 969.
- 38 A. Vonarbourg, C. Passirani, P. Saulnier and J. P. Benoit, *Biomaterials* 2006, **27**, 4356.
- 39 S. M. Moghimi, A. C. Hunter and J. C. Murray, *Pharmacol. Rev.* 2001, **53**, 283.

- 40 M. T. Peracchia, C. Vauthier, D. Desmaele, A. Gulik, J. C. Dedieu, M. Demoy, J. d'Angelo and P. Couvreur, *Pharm. Res.* 1998, **15**, 550.
- 41 R. Weissleder, A. Bogdanov, E. A. Neuwelt and M. Papisov, *Adv. Drug Del. Rev.* 1995, **16**, 321.
- 42 C. Corot, P. Robert, J. M. Idee and M. Port, *Adv. Drug Del. Rev.* 2006, **58**, 1471.
- 43 C. Wilhelm, F. Gazeau, J. Roger, J. N. Pons and J. C. Bacri, *Langmuir* 2002, **18**, 8148.
- 44 C. Billotey, C. Wilhelm, M. Devaud, J. C. Bacri, J. Bittoun and F. Gazeau, *Magn. Reson. Med.* 2003, **49**, 646.
- 45 B. Obermeier and H. Frey, *Bioconjugate Chem.* 2011, **22**, 436.
- 46 K. L. Killops, L. M. Campos and C. J. Hawker, *J. Am. Chem. Soc.* 2008, **130**, 5062.
- 47 M. K. Yu, Y. Y. Jeong, J. Park, S. Park, J. W. Kim, J. J. Min, K. Kim and S. Jon, *Angew. Chem. Intl. Ed.* 2008, **47**, 5362.
- 48 C. Sun, J. S. H. Lee and M. Zhang, *Adv. Drug Del. Rev.* 2008, **60**, 1252.
- 49 J. R. McCarthy and R. Weissleder, *Adv. Drug Del. Rev.* 2008, **60**, 1241.
- 50 T. R. Daniels, E. Bernabeu, J. A. Rodriguez, S. Patel, M. Kozman, D. A. Chiappetta, E. Holler, J. Y. Ljubimova, G. Helguera, and M. L. Penichet, *Biochim. Biophys. Acta* 2012, **1820**, 291.
- 51 T. R. Daniels, T. Delgado, J. A. Rodriguez, G. Helguera and M. L. Penichet, *Clinical Immunology* 2006, **121**, 144.
- 52 W. Arap, R. Pasqualini and E. Ruoslahti, *Science* 1998, **279**, 377.
- 53 W. Cai, D. W. Shin, K. Chen, O. Gheysens, Q. Cao, S. X. Wang, S. S. Gambhir and X. Chen, *Nano Lett.* 2006, **6**, 669.
- 54 H. Mao, W. Chen, S. Laurent, C. Thirifays, C. Burtea, F. Rezaee and M. Mahmoudi, *Colloids Surf. B: Biointerfaces* 2013, **109**, 212.
- 55 D. Walczyk, F. B. Bombelli, M. P. Monopoli, I. Lynch and K. A. Dawson, *J. Am. Chem. Soc.* 2010, **132**, 5761.
- 56 C. D. Walkey, J. B. Olsen, H. Guo, A. Emili and W. C. W. Chan, *J. Am. Chem. Soc.* 2012, **134**, 2139.
- 57 C. D. Walkey and W. C. W. Chan, *Chem. Soc. Rev.* 2012, **41**, 2780.
- 58 T. A. Larson, P. P. Joshi, and K. Sokolov, *ACS Nano* 2012, **6**, 9182.
- 59 H. Lee, E. Lee, D. K. Kim, N. K. Jang, Y. Y. Jeong and S. Jon, *J. Am. Chem. Soc.* 2006, **128**, 7383.
- 60 R. Weissleder, M. Nahrendorf and M. J. Pittet, *Nat. Mater.* 2014, **13**, 125.
- 61 P. Aggarwal, J. B. Hall, C. B. McLeland, M. A. Dobrovolskaia and S. E. McNeil, *Adv Drug Deliv Rev.* 2009, **61**, 428.
- 62 Y. Ye, and X. Chen, *Theranostics* 2011, **1**, 102.
- 63 K. Temming, R. M. Schifflers, G. Molema, and R. J. Kok, *Drug Resist. Update.* 2005, **6**, 381.
- 64 J. Huang, L. Wang, R. Lin, A. Y. Wang, L. Yang, M. Kuang, W. Qian and H. Mao, *ACS Appl. Mater. Interfaces* 2013, **5**, 4632.
- 65 T. Rojanarata, P. Opanasopit, T. Ngawhirunpat and C. Saehuan, *Talanta* 2010, **82**, 444.
- 66 B. Romberg, J. M. Metselaar, T. deVringer, K. Motonaga, J. J. K. Bosch, C. Oussoren, G. Storm and W. E. Hennink, *Bioconjugate Chem.* 2005, **16**, 767.
- 67 J. C. Y. Chan, K. Burugapalli, H. Naik, J. L. Kelly and A. Pandit, *Biomacromolecules* 2008, **9**, 528.
- 68 R. E. Brown, K. L. Jarvis and K. J. Hyland, *Anal. Biochem.* 1989, **180**, 136.
- 69 A. Henning, A. Hoffmann, H. Borcherdig, T. Thiele, U. Schedler, and U. Resch-Genger, *Anal. Chem.* 2011, **83**, 4970.



80x36mm (300 x 300 DPI)